ISSN 1392-2114 ULTRAGARSAS (ULTRASOUND), Vol.63, No.2, 2008.

Modelling of Lamb waves in a rectangular plate

L. Mažeika, A. Maciulevičius, R. Kažys

Prof. K. Baršauskas Ultrasound Institute,
Kaunas University of Technology

Abstract

Interpretation of the ultrasonic signals measured in guided waves applications usually are more complicated comparing to conventional ultrasonic inspection mainly due to existence of different wave modes and multiple reflections. The objectives of this work are to investigate the regularities of Lamb waves generated by transducer arrays in rectangular steel plate and to develop the model enabling to predict the waveforms of the signals in such a way simplifying the interpretation of inspection results. The directivity patterns of small shear wave transducer have been investigated in details using the finite element modelling. It was demonstrated that the directivity patterns of A_0, S_0 ir S_H mode waves coinside with the theoretical directivity pattern of the dipole. The uncertainties of this coincidence have been evaluated. The relatively simple method have been developed for calculation of the signals reflected in the rectangular plate taking into account group and phase velocities of guided waves and losses caused by the diffraction. The model enables to predict the signals generated by a single transducer or transducer array attached at arbitrary selected point on a steel plate.
Keywords: Wave reflection, transducer array, Lamb waves, directivity pattern, modelling.

Introduction

The application of guided waves for inspection of large and elongated industrial components is quite attractive mainly to their property to propagate long distances with relatively small losses [1-2]. On the other hand this leads to the presence of multiple reflections in the received signals. Together with a multimode character of guided waves this complicates understanding of the obtained results and usually requires an additional modelling for a better interpretation [3]. Such a problem arise in the inspection of the sheet piles or steel plates when the signals many times reflected across the objects mask the important reflection coming from the front part of the object. The analysis of the different configuration transducers array has shown that almost in all cases the several modes are generated propagating in different directions depending on the complicated multi-lobe directivity patterns [4]. The calculated directivity patterns partially explain the properties of transducer arrays, but interpretation of the signals is still complicated. In order to relate the parameters of the transducer arrays to the regularities of measured signals the objective of work presented is to investigate the regularities of Lamb waves generated by transducer arrays in a rectangular steel plate and to develop the model enabling to predict the waveforms of the signals in such a way simplifying their interpretation.

The Lamb waves generated by a shear displacement point source

In many types of long range ultrasonic inspection the shear type transducers are used [1, 2, 5]. Anyway, the investigation carried out demonstrated that such a transducer generates several wave modes also [4]. So, the objective of the first stage of investigation was to analyse the directivity patterns of the shear type source in more details and to obtain accurate analytical estimations of directivity patterns which can be used for a prediction of the measured signals. In order to obtain accurate amplitudes of the generated Lamb wave modes the numerical simulation has been carried out.

The investigation was performed using a finite element 3D model of the aluminium plate (Fig.1a). The dimensions of the plate are 0.5x0.5m and the thickness 10mm. The parameters of the aluminium used in the modelling are: the density ρ_{Al} - 2700 kg/m^3, the Young modulus E_{Al}, - 70GPa, the Poisson's ratio ν – 0.33. The relatively fine sampling in the space domain has been used. The grid step was 1.5 mm.

In order to have a sufficient spatial resolution for determination of the amplitudes of different wave modes the relative short excitation pulse have been used – only the 2 periods burst possessing the Gaussian envelope and the frequency 70 kHz. The waveform of the excitation signal is presented also in Fig.1b. The point source of a shear excitation force was applied at the centre of the aluminium plate oriented along *y* axis.

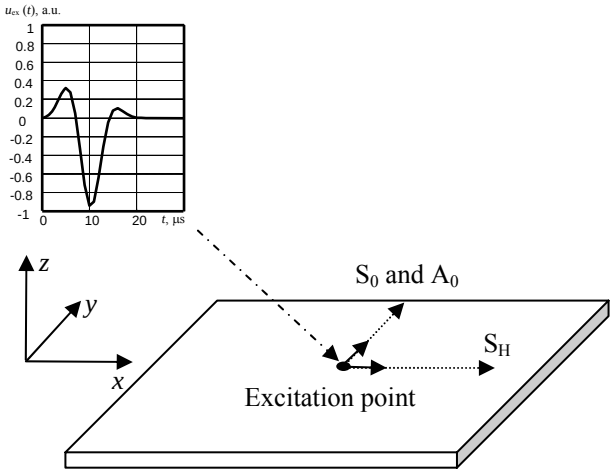

Fig. 1. **Investigation of a directivity pattern of a point shear type transducer in an aluminium plate**.

The simulation of wave propagation was performed in the time interval 0-100 μs. The obtained distribution of the

particle velocity modulus on the surface of the plate $v_{t=50}(x,y)=\sqrt{v_{x,t=50}^2(x,y)+v_{y,t=50}^2(x,y)+v_{z,t=50}^2(x,y)}$ at the time instants 50 μs demonstrates presence of several wave modes propagating with different velocities (Fig.2). The v_x, v_y, v_z are the components of the particle velocity along *x*, *y* and *z* axes.

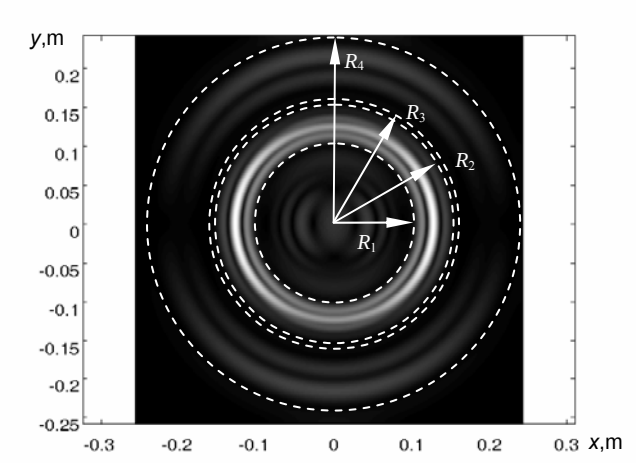

Fig. 2. **The distribution of the modulus of the particle velocity *v* of at the time instance 50 μs after the shear type excitation**

There can be observed two regions of propagating waves. Closest to the centre possibly correspond to the propagating A_0 and S_{H0} modes of Lamb waves. They possess similar group velocities – correspondingly 3176 m/s and 2955 m/s. The furthest from the centre correspond to the propagating S_0 mode with the group velocity 5166m/s. The velocities were obtained from the dispersions curves. In order to select the space domain corresponding to the desired wave mode several ring shape space windows have been calculated. The first one, limited by the radii R_1 and R_2 correspond to the position both A_0 and S_{H0} mode waves and is defined by

$$\begin{aligned} R_1 &= c_{\mathrm{G,A0}} \cdot (t_a - t_{ex}), \\ R_2 &= c_{\mathrm{G,A0}} \cdot t_a, \end{aligned} \tag{1}$$

where $c_{\mathrm{G,A0}}$ is the group velocity of A_0 mode waves, $t_a = 50\mu s$ is the time instance under analysis, t_{ex} is the duration of the excitation pulse. The second space window limited by radii R_3 and R_4 corresponds to the position both S_0 and S_{H0} mode waves and is defined by

$$\begin{aligned} R_3 &= c_{\mathrm{G,S0}} \cdot (t_a - t_{ex}), \\ R_4 &= c_{\mathrm{G,S0}} \cdot t_a, \end{aligned} \tag{2}$$

where $c_{\mathrm{G,S0}}$ is the group velocity of S_0 mode waves.

For more accurate determination of the directivity patterns *a priori* knowledge about properties of different modes have been used. In the asymmetric A_0 mode mainly the vertical v_z components dominate. Correspondingly, in the symmetric S_0 mode dominates the particle velocity component normal to the wavefront and in the S_{H0} - the tangential to the wavefront. Assuming that the wavefront should be circular in the case under analysis the normal v_N and tangential v_T components of particle velocity are by

$$\begin{aligned} v_N(x,y) &= v_x(x,y)\cdot\cos(\alpha) + v_y(x,y)\cdot\sin(\alpha), \\ v_T(x,y) &= -v_x(x,y)\cdot\sin(\alpha) + v_y(x,y)\cdot\cos(\alpha), \end{aligned} \tag{3}$$

where $\alpha = \arctan(x/y)$. The directivity patterns of different mode waves then can be obtained by

$$d_{A_0}(\alpha_k) = \max_{R_1<R<R_2}\left\{\max_{a_1<a<a_2}\left(\left|v_{z,t=50}(x,y)\right|\right)\right\}, \tag{4}$$

$$d_{S_0}(\alpha_k) = \max_{R_3<R<R_4}\left\{\max_{a_1<a<a_2}\left(\left|v_{N,t=50}(x,y)\right|\right)\right\}, \tag{5}$$

$$d_{S_{H0}}(\alpha_k) = \max_{R_1<R<R_2}\left\{\max_{a_1<a<a_2}\left(\left|v_{T,t=50}(x,y)\right|\right)\right\}, \tag{6}$$

where $d_{A_0}(\alpha_k)$, $d_{S_{H0}}(\alpha_k)$, $d_{S_0}(\alpha_k)$ are the corresponding directivity patterns of the A_0, S_{H0} and S_0 modes, $a_k = (k-1)\cdot\Delta a$, $k = 1 \div K$, $\Delta a = 2\pi/(K-1)$, K is the number point in the directivity pattern. In our case the angular step of the calculated directivity pattern was 5°.

The obtained directivity patterns are presented in Fig.3 – 5 by dots. As can be seen all of them possess two lobes with opposite phases. In the front and backward directions both A_0 and S_0 modes are generated. The shear horizontal mode waves are generated mainly in lateral directions.

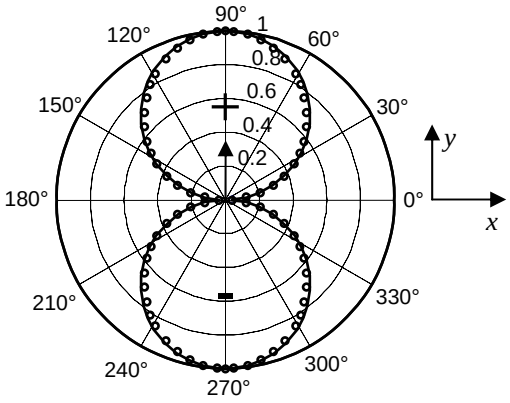

Fig. 3. **The directivity pattern $d_{A_0}(a)$ of the A_0 mode wave in the case of the tangential excitation obtained from the results of the finite element modelling (dots). The direction of the excitation force is denoted by the arrow.**

The directivity patterns obtained from the numerical modelling are very similar to the typical directivity pattern of the dipole, which usually is expressed by sinus function in polar coordinates. In order to verify this assumption the directivity patterns of all three modes have been calculated using the expression describing the directivity pattern of a dipole:

$$\begin{aligned} d_{A_0,T}(a) &= \sin(a), \\ d_{S_0,T}(a) &= \sin(a), \\ d_{S_{H0},T}(a) &= \cos(a) \end{aligned}$$

were $a = 0 \div 2\pi$.

The theoretical directivity patterns are presented in Fig.3-5 by the solid line. The deviations of the numerical directivity pattern with respect to the theoretical one are calculated according to

$$\Delta_{A_0}(a) = \left(d_{A_0}(a) - d_{A_0,T}(a)\right)\cdot 100\%, \quad (7)$$

$$\Delta_{S_0}(a) = \left(d_{S_0}(a) - d_{S_0,T}(a)\right)\cdot 100\%, \quad (8)$$

$$\Delta_{S_H}(a) = \left(d_{S_H}(a) - d_{S_H,T}(a)\right)\cdot 100\%. \quad (9)$$

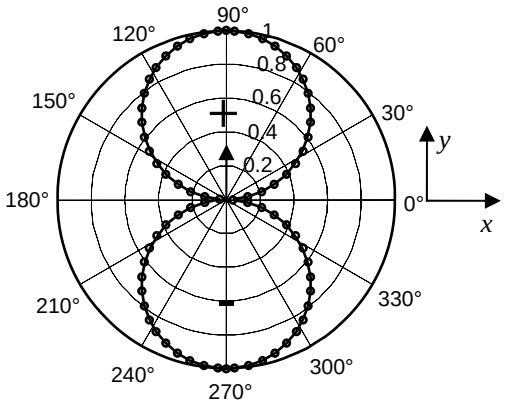

Fig. 4. **The directivity pattern $d_{S_0}(a)$ of S_0 mode wave in the case of the tangential excitation obtained from the results of the finite element modelling (dots). The direction of the excitation force is denoted by the arrow.**

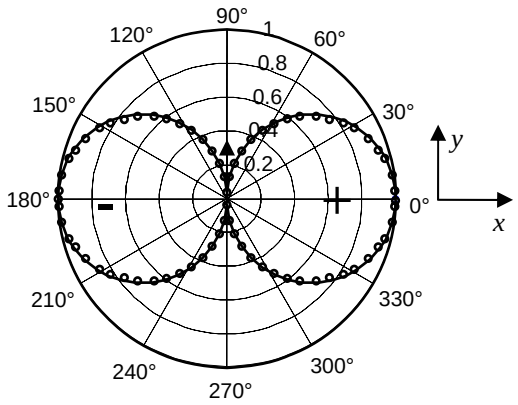

Fig. 5. **The directivity pattern $d_{S_H}(a)$ of S_H mode wave in the case of the tangential excitation obtained from the results of the finite element modelling (dots). The direction of the excitation force is denoted by the arrow.**

The obtained deviations are presented in Fig. 6-8. As can be seen from the results obtained the maximal deviation does not exceed 3%. It also can be observed that the deviation of S_0 mode directivity pattern is essentially smaller comparing to the other modes. It can be explained by the fact that the accuracy of the numerical modelling essentially depends on the step of the sampling in the space domain or the numerical grid step. The sampling step is related to the wavelength of the wave under investigation. Usually it is recommended to have 15-20 steps in the wavelength. In the case of our simulation the step of the numerical grid was set to 1.5 mm. Taking into account the wavelength of the A_0, S_0 and S_{H0} modes at the central frequency this leads to the approximately 20 steps in the wavelength of the slowest A_0 mode wave. On the other hand the excitation signal was relatively wide band.

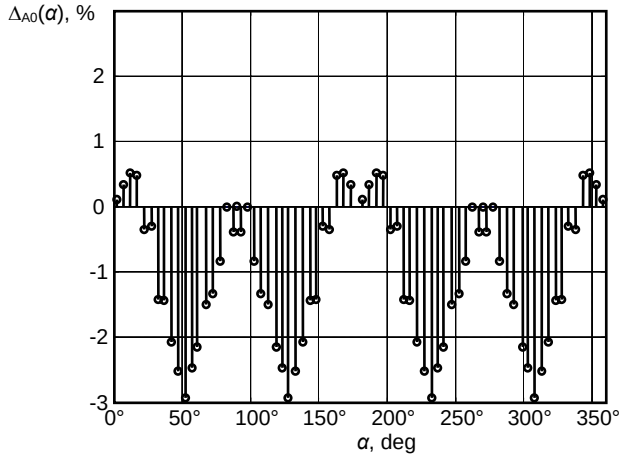

Fig. 6. **The deviation of the modelled directivity pattern $\Delta_{A_0}(a)$ of A_0 wave mode with respect to theoretical one.**

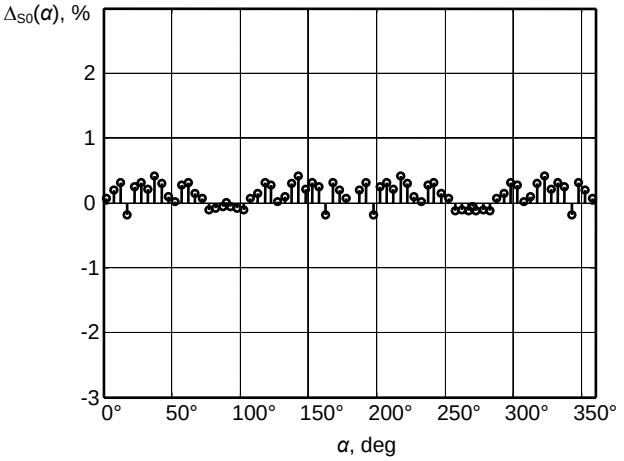

Fig. 7. **The deviation of the modelled directivity pattern $\Delta_{S_0}(a)$ of S_0 wave mode with respect to theoretical one.**

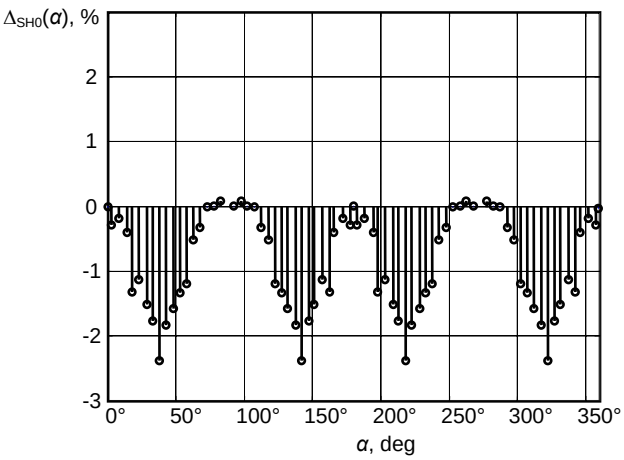

Fig. 8. **The deviation of the modelled directivity pattern $\Delta_{S_H}(a)$ of S_H wave mode with respect to theoretical one.**

So, the simulation of the shortest waves can be affected by the numerical grid what leads to the distortions and as a consequence to a bigger deviation. The S_0 mode wave is fastest one, possess the longest wavelength and therefore should have smallest distortions caused by the numerical grid.

The presented directivity patterns are normalized and of course have different normalization values. These normalization values in general enable to compare the absolutes amplitudes of the generated waves in the case of the ideal shear type excitation. The higher efficiency possess the shear horizontal Lamb wave mode. The amplitudes of the generated Lamb wave modes normalized with respect to bigger one (shear horizontal) are: $d_{N,\max,S_{H0}} = 1$; $d_{N,\max,A_0} = 0.59$; $d_{N,\max,S_0} = 0.27$.

The algorithm of calculation of the signals of reflected guided waves in a rectangular plate

The calculated directivity patterns demonstrates that even in the case of ideal shear type excitation the waves of three Lamb wave modes are generated. This fact complicates the development of the transducer arrays possessing the required directivity pattern and in principle does not allow generation of only one type of waves. This problem becomes even more complicated when the measurements are performed on the real object with boundaries, because the signals of different mode waves reflected by boundaries at different distances overlap on each other in such a way complicating understanding and interpretation of the observed signals.

So, the objective of this part of investigation was development of the model which enables to predict the signals exploiting the directivity patterns of the transducer arrays and using the information about the object geometry.

The technique for calculation of directivity patterns of transducer arrays having different configurations was described in [4].

The steel plate with dimensions Dx_{pl} by Dy_{pl} was selected as an object for model development. The algorithm is based on the determination of the paths of different reflected signals and then calculation of the propagation time t_{Rn} and the amplitude A_{Rn} of each reflection, where $n = 1 \div N$, N is the total number of reflections which were taken into account. Two types of reflections were analysed: a corner reflection and planar reflections from plate boundaries. It was assumed that the transmitting and receiving arrays can be placed at different positions, but possess the same directivity pattern.

The explanation of the planar reflections which were analysed is presented in Fig. 9.

The delay time of the reflected signal is calculated according to:

$$t_{R1} = \frac{\sqrt{\left(x_{rfl} - x_R\right)^2 + \left(y_T - y_R\right)^2}}{c}, \qquad (10)$$

$$x_{rfl} = Dx_{pl} - x_T,\ A_{R1} = \left[DP\left(\alpha_{RP}\right)\right]^2, \qquad (11)$$

where DP is the directivity pattern of the transducer array, $\alpha_{RP} = \arctan\left(\frac{\left(y_T - y_R\right)}{\left(x_{rfl} - x_R\right)}\right)$, c is the group velocity of the wave mode under analysis. It is assumed that the directivity patterns of the transmitter and receiver are the same and symmetric with respect to the x axis.

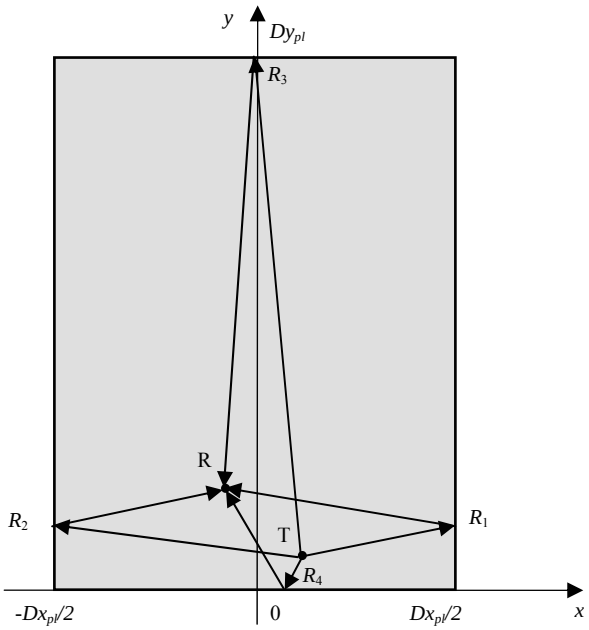

Fig. 9. **Explanation of the direct reflections from the planar reflections**

The other planar reflections are calculated according to:

$$t_{R2} = \frac{\sqrt{\left(x_{rfl} - x_R\right)^2 + \left(y_T - y_R\right)^2}}{c}, \qquad (12)$$

$$x_{rfl} = Dx_{pl} - x_T,\ A_{R2} = \left[DP\left(\alpha\right)\right]^2, \qquad (13)$$

$$t_{R3} = \frac{\sqrt{\left(x_{rfl} - x_R\right)^2 + \left(y_T - y_R\right)^2}}{c}, \qquad (14)$$

$$x_{rfl} = Dx_{pl} - x_T,\ A_{R3} = \left[DP\left(\alpha\right)\right]^2, \qquad (15)$$

$$t_{R4} = \frac{\sqrt{\left(x_{rfl} - x_R\right)^2 + \left(y_T - y_R\right)^2}}{c}, \qquad (16)$$

$$x_{rfl} = Dx_{pl} - x_T,\ A_{R4} = \left[DP\left(\alpha\right)\right]^2. \qquad (17)$$

The corner reflections (Fig. 10.) are given by

$$t_{R5} = \frac{\sqrt{\left(Dx_{pl}/2 - x_T\right)^2 + \left(y_T\right)^2}}{c} + \frac{\sqrt{\left(Dx_{pl}/2 - x_R\right)^2 + \left(y_R\right)^2}}{c}, \qquad (18)$$

$$A_{R5} = DP\left(\alpha_{T5}\right) \cdot DP\left(\alpha_{R5}\right), \qquad (19)$$

$$\alpha_{T5} = \arctan\left(\frac{(y_T)}{(Dx_{pl}/2 - x_T)}\right), \quad (20)$$

$$\alpha_{R5} = \arctan\left(\frac{(y_R)}{(Dx_{pl}/2 - x_R)}\right), \quad (21)$$

$$t_{R6} = \frac{\sqrt{(-Dx_{pl}/2 - x_T)^2 + (y_T)^2}}{c} + \frac{\sqrt{(-Dx_{pl}/2 - x_R)^2 + (y_R)^2}}{c}, \quad (22)$$

$$A_{R6} = DP(\alpha_{T6}) \cdot DP(\alpha_{R6}), \quad (23)$$

$$\alpha_{T6} = \arctan\left(\frac{(y_T)}{(-Dx_{pl}/2 - x_T)}\right), \quad (24)$$

$$\alpha_{R6} = \arctan\left(\frac{(y_R)}{(-Dx_{pl}/2 - x_R)}\right), \quad (25)$$

$$t_{R7} = \frac{\sqrt{(Dx_{pl}/2 - x_T)^2 + (Dy_{pl} - y_T)^2}}{c} + \frac{\sqrt{(Dx_{pl}/2 - x_R)^2 + (Dy_{pl} - y_R)^2}}{c}, \quad (26)$$

$$A_{R7} = DP(\alpha_{T7}) \cdot DP(\alpha_{R7}), \quad (27)$$

$$\alpha_{T7} = \arctan\left(\frac{(Dy_{pl} - y_T)}{(Dx_{pl}/2 - x_T)}\right), \quad (28)$$

$$\alpha_{R7} = \arctan\left(\frac{(Dy_{pl} - y_R)}{(Dx_{pl}/2 - x_R)}\right), \quad (29)$$

$$t_{R8} = \frac{\sqrt{(Dx_{pl}/2 - x_T)^2 + (Dy_{pl} - y_T)^2}}{c} + \frac{\sqrt{(Dx_{pl}/2 - x_R)^2 + (Dy_{pl} - y_R)^2}}{c}, \quad (30)$$

$$A_{R8} = DP(\alpha_{T8}) \cdot DP(\alpha_{R8}), \quad (31)$$

$$\alpha_{T8} = \arctan\left(\frac{(Dy_{pl} - y_T)}{(-Dx_{pl}/2 - x_T)}\right), \quad (32)$$

$$\alpha_{R8} = \arctan\left(\frac{(Dy_{pl} - y_R)}{(-Dx_{pl}/2 - x_R)}\right). \quad (33)$$

It was assumed that corners reflect all types of waves uniformly in all directions, so the directivity pattern of the corner reflector was not taken into account. The mode conversion of the wave was not analysed also.

In the next stage the arrival times of the multiple reflections are calculated for each of the planar reflections. The arrival times of multiple reflections are given by

$$\begin{aligned} t_{R1,m} &= \text{ceil}(m/2)\cdot t_{R1} + \text{floor}(m/2)\cdot t_{R2} \\ t_{R2,m} &= \text{ceil}(m/2)\cdot t_{R2} + \text{floor}(m/2)\cdot t_{R1} \\ t_{R3,m} &= \text{ceil}(m/2)\cdot t_{R3} + \text{floor}(m/2)\cdot t_{R4} \\ t_{R4,m} &= \text{ceil}(m/2)\cdot t_{R4} + \text{floor}(m/2)\cdot t_{R3} \end{aligned}, \quad (34)$$

where the functions ceil() and floor() denote rounding corresponding towards plus infinity and minus infinity.

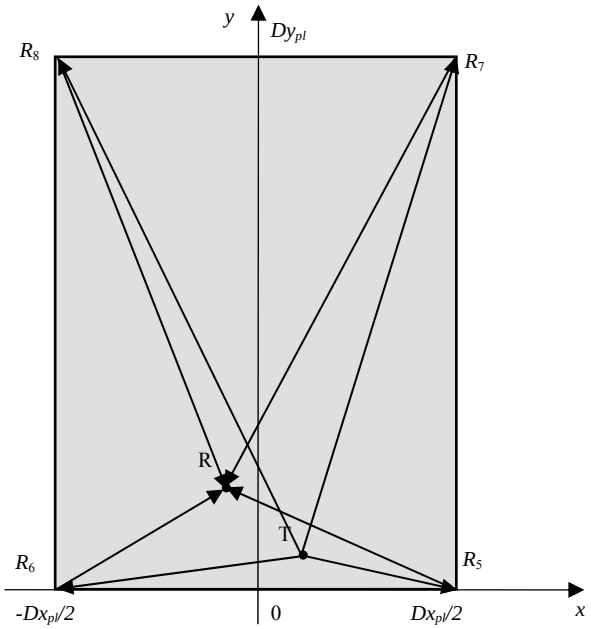

Fig. 10. **Explanation of the corner reflections**

All these procedures are repeated separately for each of the modes. As a result the set of the reflections $\{t_n, A_n\}$ is obtained. Using this set the reflected signal is calculated according to

$$u(t) = \sum_{n=1}^{N} K_{\text{mode}} \cdot K_{n,Dst} \cdot A_n \cdot u_{ref}(t - t_n)$$

where $K_{n,Dst} = \frac{1}{c \cdot t_n}$ is the coefficient which takes into account reduction of the amplitude of the propagating wave due to diffraction, K_{mode} is the coefficient which takes into account amplitude difference of the excited Lamb waves modes.

The phase shift caused by the difference of the group and phase velocities is taken into account by the modification of the reference signal and was defined in [4]

The calculation of the modeled signals of reflected guided waves in a rectangular plate

The measurement on the steel plate having the length 4m, width 2m and thickness 10mm was investigated using the model developed. The array consisting of 8 shear waves transducers, with the spacing $\lambda_{S_0}/2$ along *x* axis and λ_{A_0} along *y* axis A_0 was used (Fig. 11). The $\lambda_{S_0}, \lambda_{A_0}$ are the wavelengths of the S_0 and A_0 mode waves at the frequency 70 kHz. The shear wave excitation transducers were assumed to be oriented along *y* axis. The velocities of the Lamb wave modes propagating in the plate under analysis are presented in Table 1. The directivity pattern of the investigated transducer array is

presented in Fig.12. As can be seen strongest the A_0 mode wave are generated in the front direction and S_{H0} in lateral directions. The generation of the S_0 mode waves is not so strong, but the directivity pattern possesses multiple, almost uniformly distributed lobes.

Table 1. **The phase and group velocities of Lamb waves used in the modelling**

	c_{phase}, (m/s)	c_{group}, (m/s)
A_0	2340	3176
S_0	5306	5166
S_{H0}	2955	2955

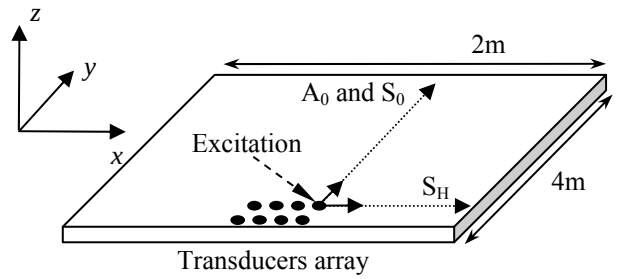

Fig. 11. **The investigated plate with denoted position of the transducer array**

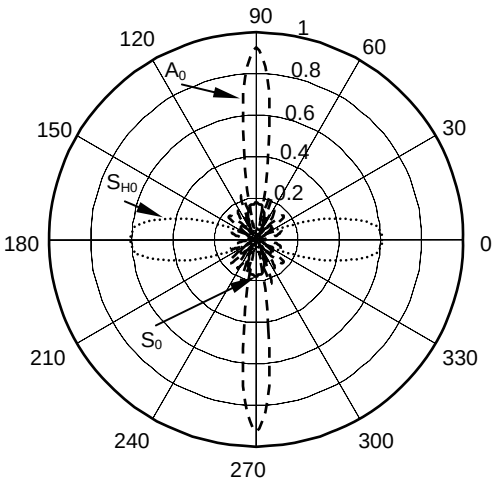

Fig. 12. **The directivity pattern of two rows (2x4) transducer array**.

The signal calculated using the model developed is presented in Fig. 13. As can be seen it contains many different multiple reflections. It is difficult to relate them to some propagating mode waves and it can be done only using obtained by the data modelling. The explanation of the identified reflections is shown in Fig. 13. The first pulse in the signal corresponds to the interference of the signals of all three modes reflected by the back edge of the plate. The multiple reflections of the S_{H0} across the plate can be observed also. Only one signal reflected by the front edge of the plate can be observed and it corresponds to A_0 Lamb mode wave. The signals of the S_0 mode possess an essentially smaller amplitude and in real measurements possibly are at the noise level.

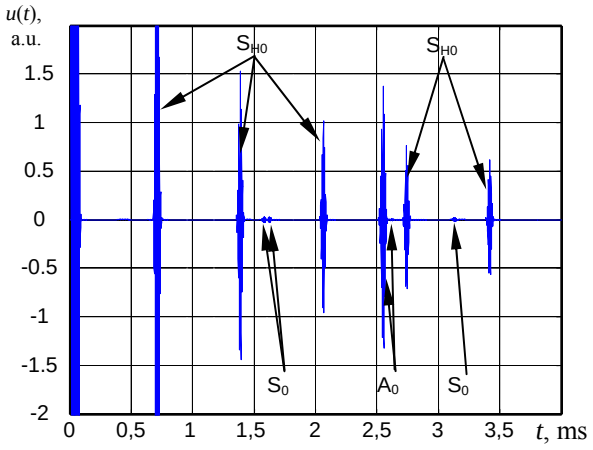

Fig. 13. **The signals, reflected in a rectangular plate.**

Discussion

It is necessary to point out that the presented results were obtained not taking into account the efficiency of different transducers of the array, which can be caused by a non-uniform acoustic coupling. The mode conversion signals were not included in the model also. The presence of them will lead to even more complicated signals. The pilot comparison of the modelled signals with the experimental ones, which were not presented there and will be the subject of the next paper, demonstrates principal coincidence of the results, but for many reasons the experimental signals are even more complicated.

However, the analysis of the directivity patterns and the signals obtained using the model developed enables to analyze and understand the results of the measurements essentially better.

Conclusions

Summarizing the obtained results it can be stated that a relatively simple and flexible model for prediction of the signals in the ultrasonic long range measurements has been developed.

The investigations demonstrated that the transducers in guided wave applications operating as point sources in all cases generate several Lamb wave modes and possess the circular or the dipole type directivity patterns.

Generation of the multiple modes leads to the complicated signals, which can be understand and interpreted only using the signals predicted by 3D models.

Acknowledgements

The part of this work was sponsored by the European Union under the Framework-6 LRUCM project. The Project is coordinated and managed by TWI (UK). Ref.: Coll-CT-2005-516405.

References

1. **Mudge P. J.** Field Application of the Teletest® Long-Range Ultrasonic Testing Technique, Insight. 2001.Vol.43. P.74- 77.
2. **Cawley P., Lowe M. J. S., Alleyne D. N, Pavlakovic B. and Wilcox P.** Practical long range guided wave testing: Applications to Pipes and Rail, Mat. Evaluation. 2003. Vol.61. P. 66-74.
3. **Lee B.C. Staszewski W.J.** Lamb wave propagation modelling for damage detection: I. Two-dimensional analysis. Smart Materials and Structures. 16(2007) P.249-259.
4. **Mažeika L. Kažys R. Maciulevičius A.** Optimization of transducer arrays parameters for efficient excitation of Lamb waves. Ultrasonics. 2007. Vol. 62. No.4. P.7-15.
5. **Kwun H. Kim S.Y. Choi M.S.** Experimental study of shear horizontal wave transmission and reflection at a tee joint. Journal of the Korean Physical Society. Vol. 44. No.2. February 2004. P461-463.

L.Mažeika, A.Maciulevičius, R. Kažys

Lembo bangų signalų stačiakampėje plokštėje modeliavimas

Reziumė

Taikyti nukreiptąsias bangas apsunkina tai, kad dėl jų daugiamodiškumo, daugkartinių įvairių modų bangų atspindžių priimtus signalus sudėtinga interpretuoti. Šio darbo tikslas yra ištirti Lembo bangų žadinimo stačiakampėje plieno plokštėje ypatumus naudojant ultragarsines gardeles ir sudaryti modelį, įgalinantį prognozuoti sužadintus signalus, kad palengvėtų jų interpretacija. Baigtinių skirtumų metodu detaliai ištirtos taškinio skersinių bangų keitiklio kryptingumo diagramos. Parodyta, kad sužadintų A_0, S_0 ir S_H modų kryptingumo diagramos sutampa su teorinėmis atitinkamai orientuoto dipolio kryptingumo diagramomis. Įvertintos šio atitikimo neapibrėžtys. Sudarytas sąlygiškai paprastas atspindžių skaičiavimo stačiakampėje metalo plokštėje modelis, įvertinantis nukreiptųjų bangų sklidimo grupinius ir fazinius greičius ir nuostolius dėl refrakcijos. Modelis leidžia skaičiuoti signalus, sužadinnamus naudojant pavienius keitiklius ar laisvai pasirinktų parametrų gardeles, įtaisytas bet kurioje plokštės vietoje.

Pateikta spaudai 2008 06 26